Kinetics of the Fe-Atom Condensation Based on Fe−Concentration Measurements†

Andreas Giesen, Jürgen Herzler, and Paul Roth*

Institut für Verbrennung und Gasdynamik, Universität Duisburg-Essen, 47048 Duisburg, Germany

Received: November 8, 2002; In Final Form: April 7, 2003

The condensation of Fe atoms was studied over the temperature range of 670−1150 K at pressures between 0.3 and 0.45 bar behind incident shock waves based on Fe concentration measurements. Atomic resonance absorption spectroscopy was applied to follow Fe atoms in gas mixtures containing $Fe(CO)_5$ as iron precursor, highly diluted in argon. At the upper experimental temperature limit, the experiments showed constant Fe-atom concentration levels after decomposition of the precursor. At a lower temperature, a time dependent decrease of the Fe concentration was observed showing an inverse temperature dependency. A simplified reaction mechanism consisting of a one step decomposition of the precursor and various iron consumption reactions was proposed for the simulation of the signals. The major initial reactions for the understanding of the condensation process were found to be the formation and the decomposition of Fe_2 (see reactions R2 and R3 in the text). The rate coefficients of both reactions were determined experimentally to be $k_2 = 10^{19}$ cm^6 mol^{-2} s^{-1} and $k_3 = 10^{19.63\pm0.40}$ exp(−17800 ± 700 K/T) cm^3 mol^{-1} s^{-1} (for reactions R2 and R3, respectively).

Introduction

The magnetic and electronic properties of iron open a wide field of technical applications for iron particles. Various techniques for the synthesis of nanopowders are known[1] to which the gas-phase synthesis belongs to. It allows the production of very small particles of uniform, clean composition. For a better understanding and description of those formation processes, kinetic data are necessary.

The synthesis of iron particles via the gas-phase route is strongly controlled by the decomposition of the precursor and the kinetics of the iron cluster formation. The group of Bauer published a series of articles about different aspects of the iron particle formation. Kung and Bauer[2] presented a shock tube technique for the determination of the temperature dependency of the critical supersaturation of iron vapor by measuring the turbidity and the thermal emission of clusters as an indicator for particle formation. In a second shock tube study,[3] the homogeneous condensation was followed by turbidity measurements and a laser-schlieren technique was applied to provide rates and enthalpies of exothermic condensation reactions. The effect of the heat of condensation on the iron cluster size was investigated, too. Frurip and Bauer[4] measured the temperature dependency of critical supersaturation ratios of the iron nucleation in a shock tube by turbidity measurements and compared the results with different nucleation models. For the kinetic interpretation of the iron particle formation, Bauer and Frurip[5] presented a self-consistent kinetic model for the homogeneous nucleation of iron vapor. The model is based on rate coefficients estimated by Lennard-Jones potentials and assumed thermodynamic properties for the reverse reactions. Bauer and Wilcox[6−8] extended and applied this kinetic model to other metals and species. In flame studies of Jensen,[9] a similar kinetic model was used and applied for modeling the particle size evaluation. The aim of the kinetic studies of Bauer and Frurip[5] and Jensen[9] is to understand the growth of iron clusters neglecting the kinetics of iron precursor decomposition. Krestinin et al.[10] performed shock tube studies using iron pentacarbonyl (IPC, $Fe(CO)_5$) as iron precursor in the temperature range of 800 K < T < 1400 K. The formation and consumption of Fe atoms was observed spectroscopically, and a strong influence of intermediate species of the precursor decomposition during Fe cluster formation was found. In addition to former mechanisms, the decomposition product FeCO was considered as an important species in their reaction mechanism to explain the iron cluster formation. This model was later theoretically extended by Warnatz et al.[11] A different approach for the interpretation of Fe-consumption signals was used by Steinwandel et al.[12,13] They performed shock tube experiments using IPC as iron precursor and absorption spectroscopy for iron atom detection. For the interpretation of the measured Fe decay times, only the Smoluchowski coagulation was applied.

In the present investigation, the condensation of iron atoms was studied in a shock tube in mixtures of IPC highly diluted in argon. The formation and consumption of Fe atoms behind incident shock waves was followed by atomic resonance absorption spectroscopy (ARAS). Also molecular resonance absorption spectroscopy (MRAS) was applied to measure the side product CO during the IPC decomposition. For the interpretation of the signals, a simplified reaction mechanism is proposed which is able to describe all measured iron concentration profiles at T > 730 K.

Experimental Section

The experiments were carried out in a conventional stainless steel, pressure-driven diaphragm shock tube having an internal diameter of 80 mm, a driver section of 3.5 m, and a driven section of 6.5 m in length. Downstream of the measurement section, a tube extension of 0.5 m in length was installed to provide sufficiently long test times behind incident shock waves. The driven section can be baked out and pumped down to a

† Dedicated to Prof. Dr. Eberhard F. Wassermann on the occasion of his 65th birthday.

* To whom correspondence should be addressed. Phone: 0049-203 379 3426. Fax: 0049-203 379 3087. E-mail: roth@ivg.uni-duisburg.de.

10.1021/jp022392x CCC: $25.00
Published on Web 06/07/2003

pressure below 5×10^{-8} mbar. The gas mixtures used were prepared manometrically in a stainless steel ultrahigh vacuum vessel. The gases and liquids used were of high commercial purity: Ar ≥ 99.9999%, CO ≥ 99.997%, and $Fe(CO)_5$ ≥ 99.5%. The IPC, which is liquid at room temperature, was injected in a separate stainless steel vessel and afterward freezed and pumped for degassing.

The Fe-atom resonance absorption diagnostic ($\lambda = 271.9$ nm) consists of a pulsed Fe-hollow cathode lamp, the optical path length, a 0.25 m Jarrel-Ash monochromator, and a photomultiplier. Perpendicular to the Fe-ARAS system, the CO-MRAS diagnostic ($\lambda = 151$ nm) consisting of a microwave excited discharge lamp, a 0.5 m McPherson vacuum ultraviolet monochromator, and a solar blind photomultiplier was arranged. The lamp was operated with a flowing gas mixture of 1% CO_2 in He maintained at a constant pressure of 6 mbar and a microwave power of about 45 W. Both diagnostics require calibration due to the unknown spectral profiles of these line emission−line absorption techniques. Therefore, a series of shock-wave experiments with known concentrations of Fe and CO have been performed to relate the measured absorptions to the corresponding concentrations. The CO calibration is based on 0.5−500 ppm CO/Ar mixtures. The calibration of the Fe diagnostic was performed with mixtures of 0.1−100.0 ppm $Fe(CO)_5$ in Ar at temperatures above 1200 K. At these conditions, the Fe-atom equilibrium concentration, which is equal to the initial $Fe(CO)_5$ concentration, is established after reaction times of only a few microseconds.[14]

Results

The condensation of Fe atoms was studied behind incident shock waves in the temperature range of 670 K ≤ T ≤ 1150 K and pressures of 0.3 to 0.45 bar in gas mixtures of 30−100 ppm $Fe(CO)_5$ diluted in Argon. In all experiments, the resonance absorption of Fe atoms and CO molecules were measured simultaneously.

A typical example illustrating the temperature dependency of the Fe-atom and CO-molecule resonance absorption in a 100 ppm $Fe(CO)_5$/Argon mixture is given in Figure 1. All Fe and CO absorption profiles show a fast increase due to the thermal decomposition of IPC to form Fe atoms and CO molecules. In the case of the highest temperature of 1110 K, the Fe absorption shows after a few microseconds a constant absorption level, indicating no further reaction within 1 ms. A decrease of the experimental temperature leads to a decreasing Fe-atom absorption with an inverse temperature dependency. At temperatures below 950 K, a subsequent Fe consumption within 1 ms was measured. At the lowest temperature of 710 K, the Fe absorption level does not reach its maximum value of 0.82 absorption units. It seems that the kinetics of the precursor decomposition is no more significantly faster than the Fe consumption process. A further decrease of the experimental temperature (not shown) causes a further reduction of the Fe-absorption maximum, respectively. The simultaneously measured CO-absorption profiles (lower part of Figure 1) show a fast increase due to the decomposition of the precursor. The subsequent constant absorption levels during the whole observation time indicate the complete decomposition of the precursor and no further reaction of the CO. No time-dependent light extinction by particles was observed. The Fe concentrations seems to be too low to interfere the absorption profiles due to particle formation. Figure 2 shows a second series of absorption experiments and the corresponding Fe-concentration profiles with lower initial IPC concentration. The general behavior of the measured species

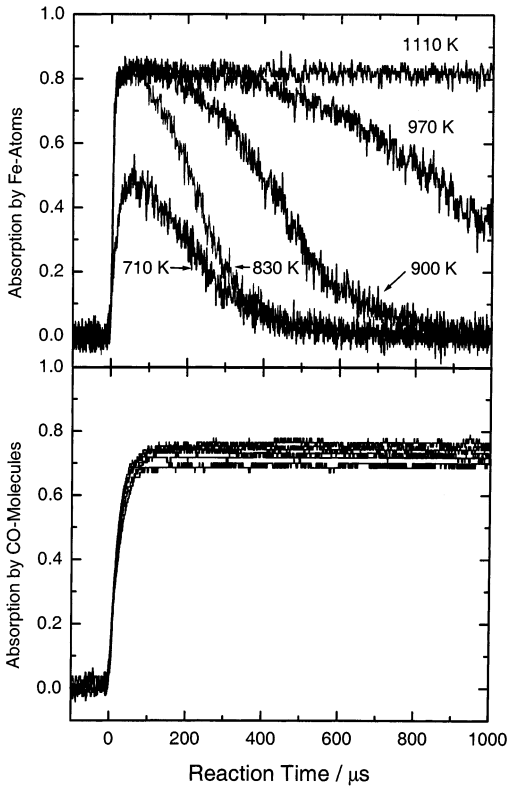

Figure 1. Fe- and CO-absorption profiles for a 100 ppm $Fe(CO)_5$/Ar mixture at different post-shock temperatures.

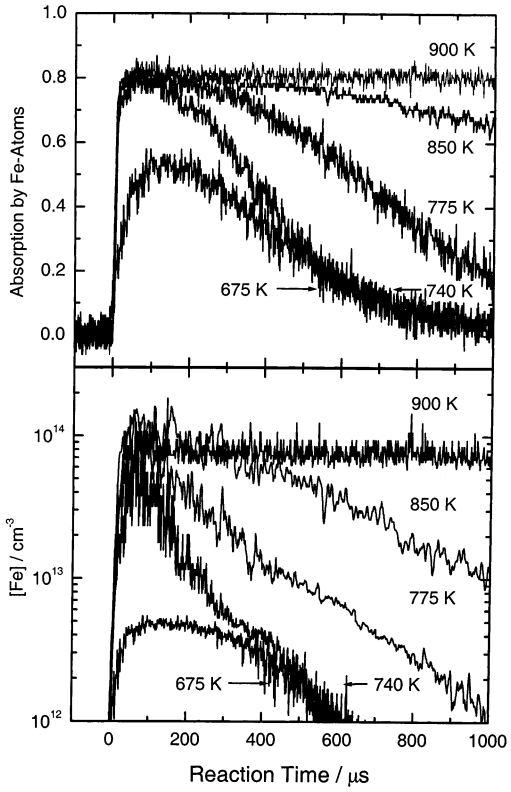

Figure 2. Fe absorption and concentration profiles for a 30 ppm $Fe(CO)_5$/Ar mixture at different post-shock temperatures.

is similar, but the temperature at which the first Fe consumption appears is shifted to lower values. In case of the 100 ppm IPC mixture, it occurs at $T \approx 1080$ K and for a 30 ppm mixture at $T \approx 940$ K.

TABLE 1: Simplified Reaction Mechanism for the Nucleation of Fe Atoms

$k_i = A \times \exp(-T_A/T)$

	reaction	rate coefficient A/cm mol s	T_A/K	ref
	$Fe(CO)_5$ Decomposition			
1	$Fe(CO)_5 \rightarrow Fe + 5\ CO$	1.9×10^9	8700	14
	Formation and Dissociation of Small Clusters			
2	$Fe + Fe + M \rightarrow Fe_2 + M$	1.0×10^{19}		this study
3	$Fe_2 + M \rightarrow Fe + Fe + M$	4.3×10^{19}	17800	this study
4	$Fe + Fe_2 + M \rightarrow Fe_3 + M$	1.0×10^{19}		estimated
5	$Fe_3 + M \rightarrow Fe_2 + Fe + M$	1.0×10^{19}	19200	estimated
6	$Fe + Fe_3 + M \rightarrow Fe_4 + M$	1.0×10^{19}		estimated
7	$Fe_4 + M \rightarrow Fe_3 + Fe + M$	5.0×10^{17}	21600	estimated
8	$Fe + Fe_4 \rightarrow Fe_5$	5.0×10^{14}		estimated
9	$Fe_5 \rightarrow Fe_4 + Fe$	1.8×10^{13}	23200	estimated
10	$Fe + Fe_5 \rightarrow Fe_6$	5.0×10^{14}		estimated
11	$Fe_6 \rightarrow Fe_5 + Fe$	1.7×10^{13}	24400	estimated
12	$Fe + Fe_6 \rightarrow Fe_7$	5.0×10^{14}		estimated
13	$Fe_7 \rightarrow Fe_6 + Fe$	1.7×10^{13}	25400	estimated
14	$Fe + Fe_7 \rightarrow Fe_8$	5.0×10^{14}		estimated
15	$Fe_8 \rightarrow Fe_7 + Fe$	1.6×10^{13}	27000	estimated
16	$Fe + Fe_8 \rightarrow Fe_9$	5.0×10^{14}		estimated
17	$Fe_9 \rightarrow Fe_8 + Fe$	1.5×10^{13}	28100	estimated
18	$Fe + Fe_n \rightarrow Fe_{n+1}$	5.0×10^{14}		estimated
	Coagulation of Clusters			
19	$Fe_2 + Fe_2 \rightarrow Fe_3 + Fe$	5.0×10^{14}		estimated
20	$Fe_2 + Fe_2 \rightarrow Fe_4$	5.0×10^{14}		estimated
21	$Fe_2 + Fe_3 \rightarrow Fe_5$	5.0×10^{14}		estimated
22	$Fe_2 + Fe_3 \rightarrow Fe_4 + Fe$	5.0×10^{14}		estimated
23	$Fe_2 + Fe_4 \rightarrow Fe_6$	5.0×10^{14}		estimated
24	$Fe_2 + Fe_5 \rightarrow Fe_7$	5.0×10^{14}		estimated
25	$Fe_2 + Fe_n \rightarrow Fe_{n+2}$	7.5×10^{14}		estimated
26	$Fe_3 + Fe_3 \rightarrow Fe_6$	5.0×10^{14}		estimated
27	$Fe_3 + Fe_4 \rightarrow Fe_7$	5.0×10^{14}		estimated
28	$Fe_3 + Fe_n \rightarrow Fe_{n+3}$	7.5×10^{14}		estimated
29	$Fe_4 + Fe_4 \rightarrow Fe_8$	7.5×10^{14}		estimated
30	$Fe_4 + Fe_5 \rightarrow Fe_9$	7.5×10^{14}		estimated
31	$Fe_4 + Fe_n \rightarrow Fe_{n+4}$	7.5×10^{14}		estimated

Discussion

The observed consumption of Fe atoms showing an inverse temperature dependency must mainly be caused by cluster formation and the thermal stability of critical clusters. Although the thermal decomposition of IPC to form Fe and CO is known to be very fast, an influence of intermediates cannot be excluded. It is accepted in the literature that the further growth of clusters to form particles mainly proceeds by coagulation with rates nearly equal to collision frequency.[15] It is expected that those coagulation processes only weakly affect the disappearance rate of Fe atoms. According to Table 1, a simplified reaction mechanism has been proposed, which contains the above-mentioned subsystems: $Fe(CO)_5$ decomposition, formation, and dissociation of small clusters and coagulation of clusters. It is easy to realize and will be shown later that the bottleneck in the above mechanism is the recombination of Fe atoms and the reverse reaction

$$Fe + Fe + M \xrightarrow{k_2} Fe_2 + M \qquad (R2)$$

$$Fe_2 + M \xrightarrow{k_3} Fe + Fe + M \qquad (R3)$$

These above reactions were identified to be most important, initiating all further Fe-condensation steps.

$Fe(CO)_5$ Decomposition Model. Woiki et al.[14] showed that the IPC decomposition proceeds via CO abstraction. At temperatures above 1000 K, the time for the total decomposition takes a few microseconds and increases significantly at the lower temperature end of this study. Figure 3 shows Fe and corresponding CO concentration profiles of an experiment at 740 K (grey line). The Fe concentration does not reach its maximum value of 1.24×10^{14} cm^{-3}, indicating that the decomposition of IPC is not fast enough compared to the consumption process. The maximum concentration of iron atoms can be 1−3 orders of magnitude lower than the initial iron pentacarbonyl concentration.[10] Therefore, strong interactions of the intermediate species on the iron cluster formation are most probable for these reaction conditions. For their consideration, a detailed knowledge about the kinetics of the IPC decomposition is necessary. At elevated temperatures, no experimentally determined kinetic mechanism for the various steps of $Fe(CO)_5$ decomposition is available in the literature. Lewis et al.[16] and Didenkulova et al.[17] measured with different techniques the kinetics of the first decomposition step. Smirnov[18] measured the first step and the formation of Fe atoms in a shock tube and calculated bonding energies by using RRKM calculations. Different estimated kinetic decomposition models are available in the literature[19,20] with estimated rate coefficients based on bonding energies.

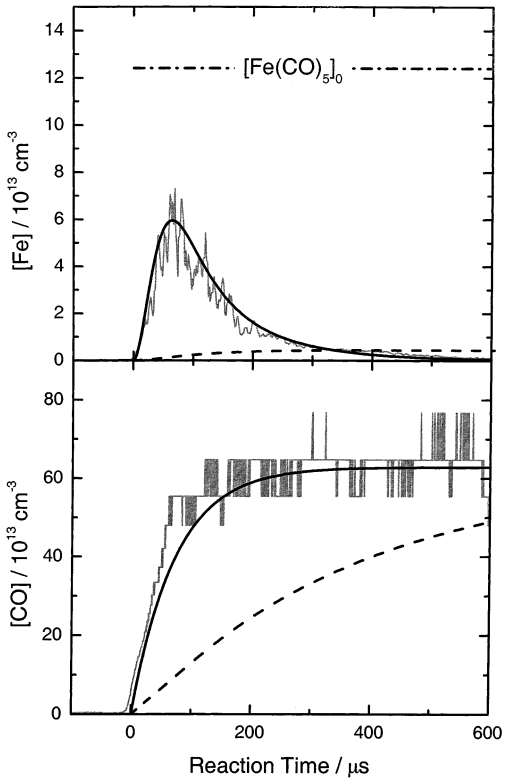

Figure 3. Fe- and CO-concentration profiles for an experiment at $T = 740$ K and 30 ppm $Fe(CO)_5$/Ar mixture. The full line is the result of a simulation using the reaction mechanism of Table 1. The dashed lines represent a simulation based on the reaction mechanism of Krestinin et al.[10]

Especially at low temperatures, an influence of the intermediate species must be considered. Krestinin et al.[10] regarded FeCO to be a very reactive species. In their reaction mechanism, the IPC decomposition is modeled in two steps. The first is the decomposition of $Fe(CO)_5$ to form FeCO and 4 CO, and in a second step, FeCO decomposes to Fe and CO. In their further mechanism, FeCO is an important species in iron cluster formation. Other intermediates were excluded to limit the complexity of the problem. We tried to model our experiments with their mechanism. In Figure 3, the Fe and CO concentration profiles of an experiment at 740 K are shown. The mechanism

TABLE 2: Bond Dissociation Energies for the Abstraction of CO from $Fe(CO)_n$ in kJ/mol

$n=1$	$n=2$	$n=3$	$n=4$	$n=5$	method	ref
32 ± 12	109 ± 12	149 ± 8	138 ± 12	159 ± 12	calculation	18
29 ± 13	141 ± 8	137 ± 13	130 ± 17		calculation	21
34 ± 15	154 ± 15	122 ± 24	117 ± 37		experiment	22
				166 ± 10	experiment	16
96 ± 29	96 ± 29	135 ± 29	19 ± 39	232 ± 48	experiment	23

of Krestinin et al.[10] yields an Fe profile which is much too low and in its shape completely different from the experimental findings, see dashed line. Also the calculated CO concentration profile is significantly below the experimental line and shows a completely different time behavior, see dashed line. This illustrates that the model is unable to predict our Fe and CO profiles. Furthermore, different experimental and theoretical studies on bonding energies of iron carbonyls are available in the literature, see Table 2. The values scatter very much, but a certain tendency can be observed. The first decomposition step seems to have the highest bonding energy. It is followed by three steps with comparable reaction enthalpies, whereas the reaction enthalpy of the last step is significantly lower. If this small bonding energy for FeCO is correct, it will become a minor species and the other iron carbonyls $Fe(CO)_x$ are likely to have a longer lifetime and may have a stronger influence and should be implemented too.

In this study, we have restricted ourself, on the kinetic interpretation of experiments with fast IPC decomposition. In the mechanism of Table 1, the decomposition of IPC was therefor modeled by the simplified one step reaction mechanism of Woiki et al.[14]

$$Fe(CO)_5 \xrightarrow{k_1} Fe + 5\ CO \qquad (R1)$$

The full lines in Figure 3 represent a simulation using the reaction mechanism of Table 1 based on the one step IPC decomposition. Both, the Fe and the CO formation process are represented well, showing the applicability of this simplified model.

Formation and Dissociation of Small Clusters. A major Fe-cluster growth mechanism is considered to be a process of Fe addition to iron clusters. The formation and removal of clusters is represented by reactions R2−R18 and is initiated by R2 and R3

$$Fe + Fe + M \xrightarrow{k_2} Fe_2 + M \qquad (R2)$$

$$Fe_2 + M \xrightarrow{k_3} Fe + Fe + M \qquad (R3)$$

The rate coefficient of the exothermic formation reaction R2 was determined by fitting the decay of an experiment at conditions, where the reverse reaction is negligible. The value obtained is $k_2 = 1.0 \times 10^{19}$ cm^6 mol^{-2} s^{-1}, which is in quite good agreement with the theoretically determined value of Bauer and Frurip ($\approx 1.7 \times 10^{19}$ cm^6 mol^{-2} s^{-1}).[5] The rate coefficients for the other reactions of single clusters with Fe atoms were estimated to be of the same magnitude like R2 and were defined to be $k = 1.0 \times 10^{19}$ cm^6 mol^{-2} s^{-1} and 5.0×10^{14} cm^3 mol^{-1} s^{-1} for termolecular and for bimolecular reactions, respectively. The value $n = 5$ at which the transition from termolecular to bimolecular kinetics is assumed to occur is based on theoretical considerations of Jensen.[9]

With increasing temperature, the Fe-atom consumption is slowing down, indicating a strong temperature dependency of the cluster dissociation reactions. Because of a lack of thermodynamic data of Fe clusters, the equilibrium constant of the reaction between Fe atoms and Fe clusters cannot be calculated with reasonable accuracy. For Fe_2, a set of high temperature thermodynamic data is given in the Landolt−Börnstein database,[24] but the accuracy of the data and the method used to obtain them is not given. Ab initio calculations of the binding energies of Fe clusters are available[25] but no entropy data are calculated. Bauer and Frurip[5] used estimated enthalpy and entropy values to calculate equilibrium constants of iron clusters. Their theoretical considerations show that the cluster becomes more stable with increasing size, and the decomposition rate is decreasing. Jensen[9] calculated temperature-dependent equilibrium constants for small Fe clusters based on molecular properties and standard enthalpies of the reactions. The uncertainties are considered to be as high as a factor of 10.

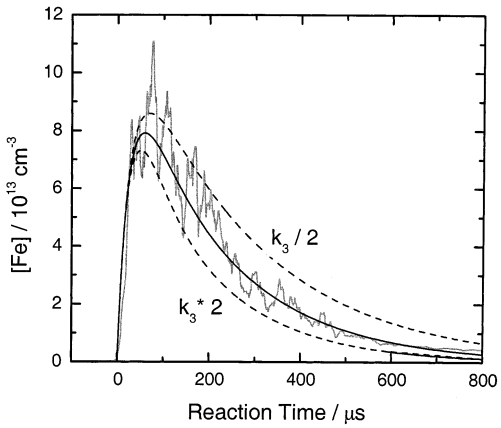

Figure 4. Fe-concentration profile for an experiment at $T = 815$ K using a 30 ppm $Fe(CO)_5$/Ar mixture. The full line represents a simulation based on the reaction mechanism of Table 1. The dashed lines show the sensitivity of the reaction mechanism on variations of k_3.

According to Table 1, rate coefficients for cluster decomposition were calculated from the rate coefficients of the forward reactions and the temperature-dependent equilibrium constants of Jensen[9] except for reaction R3. They show the same size dependent tendency like observed by Bauer and Frurip.[5] Reaction R3 is for the present experimental conditions most important to explain the measured Fe behavior. Based on the reaction mechanism of Table 1, computer simulations were performed to determine the rate coefficient k_3. Figures 3 and 4 show the result of fitting procedures for two experiments performed at different temperatures, see full lines. The rate coefficients of R3 were determined to be $k_3(740\ \text{K}) = 5 \times 10^8$ cm^3 mol^{-1} s^{-1} and $k_3(815\ \text{K}) = 2 \times 10^{10}$ cm^3 mol^{-1} s^{-1}. The dashed lines in Figure 4 indicate the sensitivity of the Fe concentration to variations of the rate coefficient k_3 by factors of 2. Best fit values of k_3 obtained from all experiments are summarized in the Arrhenius diagram of Figure 5. The data points scatter around a straight line, which can be approximated by the following Arrhenius expression:

$$k_3 = 10^{19.63 \pm 0.40} \exp(-17800 \pm 700\ \text{K/T})\ \text{cm}^3\ \text{mol}^{-1}\ \text{s}^{-1}$$

The activation energy $E_{a,3} = 148 \pm 6$ kJ/mol is of the same magnitude like the heat of reaction $\Delta H^r_{0,3} = 134$ kJ/mol of Krestinin et al.[10] It is also close to the experimentally determined bond dissociation energy of 125 kJ/mol of Moskovits et al.[26] and the reaction enthalpy of $\Delta H^r_{0,4} = 111$ kJ/mol calculated from thermodynamic data[27,24] but is significantly lower than

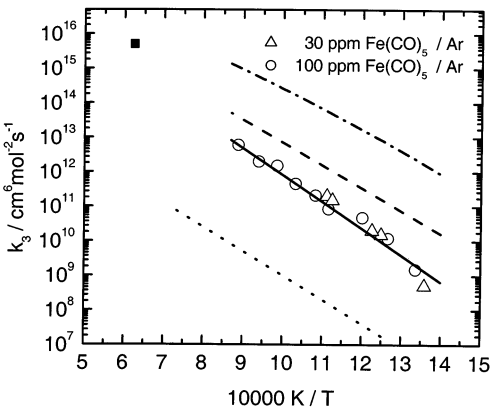

Figure 5. Arrhenius plot of the rate coefficient k_3 determined with tht reaction mechanism of Table 1 and comparison with the values determined by using the forward reaction (R2) and the temperature-dependent equilibrium constant of Jensen[9] (dashed line). The dashed−dotted is based on an equilibrium constant calculated from k_2 and the thermal properties of Fe[27] and Fe_2.[24] The dotted line represents the results of Krestinin et al.[10] The square is based on a theoretical model of Bauer and Frurip.[5]

the ab initio value of 217 kJ/mol proposed by Diéguez et al.[25] The empirical expression for the bonding energy of Freund and Bauer[3] is 146 kJ/mol, which is in very good agreement with our experimental findings.

A comparison of the present values of k_3 with data from literature is also presented in Figure 5. The result of Krestinin et al.[10] is significantly lower, see the dotted line. This is mostly due to the fact that they favor FeCO reactions to be the major cluster formation channels which is in disagreement with our observations. Bauer and Frurip estimated the coefficient at 1600 K to be $k_3(1600\ K) \approx 5.0 \times 10^{15}$ cm^3 mol^{-1} s^{-1} which is higher than our value, see the square. A calculation of the rate coefficient determined by the forward reaction R2 and the equilibrium constant of Jensen[9] is also plotted in Figure 5, see the dashed line. It shows a comparable activation energy but the absolute values differ by an order of magnitude. This corresponds to the error limits of the equilibrium constant of Jensen[9] to be about a factor of 10. The dashed−dotted line shows a second calculation based on the forward rate coefficient k_2 and an equilibrium constant determined from the thermodynamic properties of Fe[27] and Fe_2.[24] This results in a much higher rate coefficient than determined by the present experiments and is not able to describe the measured iron profiles properly. Therefore, a more detailed discussion of the thermal properties of Fe_2 must be performed.

Coagulation of Clusters. The coagulation process is considered by reactions R19−R31. For simplification, equally sized iron clusters are supposed to have the same structure and are treated as individual chemical components of the gaseous mixture. For the modeling, clusters with a size up to four atoms are considered as collision partners. The estimated rate coefficients are based on collision frequencies.

Sensitivity Analysis of the Reaction Mechanism. The influence of the various rate coefficients of the simplified reaction mechanism of Table 1 on the measured Fe concentration was studied by a detailed sensitivity analysis using SENKIN.[28] The normalized sensitivity to the measured Fe concentration is defined as

$$S_{\mathrm{Fe},i} = \frac{k_i}{[\mathrm{Fe}]} \frac{\delta[\mathrm{Fe}]}{\delta k_i}$$

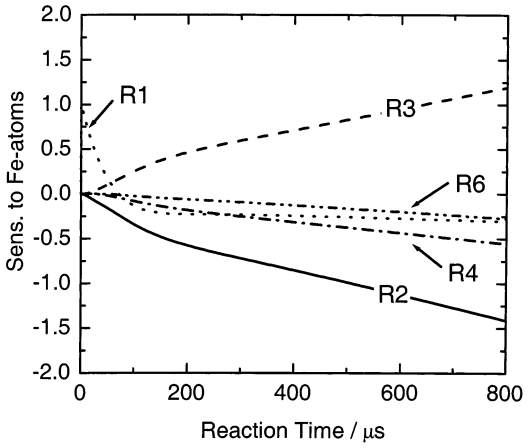

Figure 6. Normalized sensitivities of the mechanism in Table 1 showing the influence of the individual reactions on the Fe-atom concentration. The sensitivities are calculate for the reaction conditions of Figure 4.

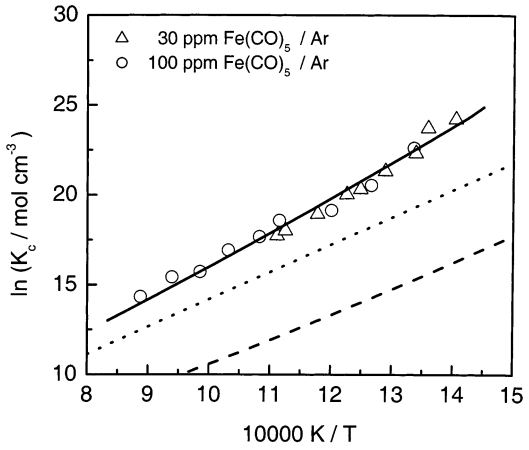

Figure 7. Equilibrium constant K_c calculated from k_2 and k_3. An estimation by Jensen[9] is represented by the dotted line. The dashed line shows K_c calculated from the thermal properties of Fe and Fe_2 with the thermodynamic data given in the literature.[24,27] The full line is calculated with the modified heat of formation for Fe_2.

A typical result of calculated sensitivities for the reaction conditions of Figure 4 is presented in Figure 6. At an early reaction time $t < 55$ μs, the IPC decomposition reaction R1 is most important. At $t > 110$ μs, its influence disappears nearly completely, and the sensitivity goes mostly to the recombination reaction R2 and the balancing dissociation of Fe_2 by reaction R3. At reaction times $t > 100$ μs, other nucleation reactions such as R4 and R6 are getting some importance. The other reactions of the mechanism of Table 1 have minor sensitivities on the time behavior of the measured Fe concentration.

Thermal Properties of Fe_2. From the kinetically determined rate coefficients k_2 and k_3 for the formation and destruction of Fe_2, its thermal properties can be estimated, although Fe_2 itself could not be measured. The ratio of the two rate coefficients is equal to the equilibrium constant K_c, which is presented as a function of temperature in Figure 7, see the points. The mean value can be approximated by

$$K_c = \frac{k_2}{k_3} = 10^{-0.63\pm0.40} \exp(17800 \pm 700\ \mathrm{K/T})\ \mathrm{cm^3\ mol^{-1}}$$

The equilibrium values calculated by Jensen[9] based on estimated partition functions are also shown as dotted line in Figure 7. The temperature dependency is similar, but the absolute value

is about a factor of 10 lower, which is within the error limits of the Jensen study. A calculation of the equilibrium constant determined from the thermodynamic data of Fe[27] and Fe_2[24] is plotted as a dashed line, which is significantly lower than our values.

The discrepancies in the equilibrium constant of Figure 7 are mostly a result of the not precisely known thermodynamic properties of Fe_2. We have therefore tried to determine the heat of formation of Fe_2 from our experimental K_c values. For this purpose, an average heat capacity and the standard entropy of Fe_2 were assumed to be $C_p = 45$ J/mol *K* and S^0 (298) = 248.3 J/mol K, respectively.[24] A best fit value for the heat of formation of Fe_2 (see solid line in Figure 7) was obtained with a value of $\Delta H_f^0 = 675 \pm 4$ kJ/mol. This value is about 6% lower than the literature value[24] and fits the experiments nearly exactly.

Conclusion

The nucleation of Fe atoms was investigated by measuring Fe-atom concentrations behind incident shock waves in $Fe(CO)_5$ mixtures highly diluted in argon at temperatures between 670 and 1150 K and pressures between 0.3 and 0.45 bar. A strong temperature dependency of the iron consumption was observed. A simplified reaction mechanism was proposed and used for the interpretation of the measured concentration profiles. The formation and the thermal stability of Fe_2 clusters is the most sensitive reaction for the modeling of nucleation. The influence of intermediate species $Fe(CO)_x$ was found to be of minor importance at temperatures $T > 730$ K.

Acknowledgment. The authors thank Natascha Schlösser for her help in performing the experiments. The financial support of the German Science Foundation DFG is gratefully acknowledged.

References and Notes

(1) Kalyanaraman, R.; Sang, Y.; Krupashankara, M. S.; Sudarshan, T. S.; Dowding, R. J. *J. Nanostruct. Mater.* **1998**, *10*, 1379.
(2) Kung, R. T. V.; Bauer, S. H. *Proc. Int. Symp. Shock Waves 8, London*, **1971**, paper No. 61.
(3) Freund, H. J.; Bauer, S. H. *J. Phys. Chem.* **1977**, *81*, 994.
(4) Frurip, D. J.; Bauer, S. H. *J. Phys. Chem.* **1977**, *81*, 1001.
(5) Bauer, S. H.; Frurip, D. J. *J. Phys. Chem.* **1977**, *81*, 1015.
(6) Wilcox, C. F., Jr.; Bauer, S. H. *J. Phys. Chem.* **1991**, *94*, 8302.
(7) Bauer, S. H.; Wilcox, C. F., Jr. *J. Phys. Chem.* **1993**, *97*, 271.
(8) Bauer, S. H.; Wilcox, C. F., Jr. *Chem. Phys. Lett.* **1995**, *232*, 253.
(9) Jensen, D. E. *J. Chem. Soc. Faraday Discuss. 2* **1980**, *76*, 1494.
(10) Krestinin, A. V.; Smirnov, V. N.; Zaslonko, I. S. *Sov. J. Chem. Phys.* **1991**, *8* (3), 689.
(11) Warnatz, J.; Behrendt, F.; Sojka, J.; Wagner, H. Gg.; Zaslonko, I. S.; Vlasov, P. A.; Karasevich, Yu. K.; Smirnov, V. N.; Starikovskii, A. Yu. *Computer Modeling of Iron Clusters Growth and Decomposition behind Shock Waves* [CD-ROM]. 3rd Workshop on Modelling of Chemical Reaction Systems. Heidelberg, Germany, 24−26 July, 1996. Also available at: http://reaflow.iwr.uni-heidelberg.de/~crs96/Program/Contrib/Paper/p53wa.pdf.
(12) Steinwandel, J.; Diez, Th.; Joos, V.; Hauser, M. *Ber. Bunsen-Ges. Phys. Chem.* **1981**, *85*, 683.
(13) Steinwandel, J. Ph.D. Thesis, Universität Stuttgart, Germany, 1979.
(14) Woiki, D.; Giesen, A.; Roth, P. *Proc. Int. Symp. Shock Waves 23* **2001**, 253−259.
(15) Friedlander, S. K. *Smoke, Dust, and Haze*, 2nd ed.; Oxford University Press: New York, 2000; p 188−221.
(16) Lewis, K. E.; Golden, D. M.; Smith, G. P. *J. Am. Chem. Soc.* **1984**, *106*, 3905.
(17) Didenkulova, I. I.; Perepletchikov, M. L.; Aleksandrov, Y. A. *Russ. J. Phys. Chem.* **1990**, *64*, 1836.
(18) Smirnov, V. N. *Kinet. Catal.* **1993**, *4*, 951.
(19) Dateo, C. E.; Gökçen, T.; Meyyappan, M. *J. Nanosci. Nanotech.* **2002**, *2*, 523.
(20) Rumminger, M. D.; Reinelt, D.; Babushock, V.; Linteris, G. T. *Combust. Flame* **1999**, *116*, 207.
(21) Ricca, A. *Chem. Phys. Lett.* **2001**, *350*, 231.
(22) Sunderlin, L. S.; Wang, D.; Squires, R. R. *J. Am. Chem. Soc.* **1992**, *114*, 2788.
(23) Engelking, P. C.; Lineberger, W. C. *J. Am. Chem. Soc.* **1979**, *101*, 5569.
(24) Landolt, H.; Börnstein, R. *Numerical Data and Functional Relationships in Science and Technology, New Series*, Vol. IV/19A1; Springer: Berlin, 1999; p 44.
(25) Diéguez, O.; Alemmany, M. M. G.; Rey, C.; Ordejón, P.; Gallego, L. J. *Phys. Rev. B* **2001**, *63*, 205407.
(26) Moskovits, M.; DiLella, D. P.; Limm, W. *J. Chem. Phys.* **1984**, *80*, 626.
(27) Chase, M. W., Jr.; Davies, C. A.; Downey, J. R., Jr.; Frurip, D. J.; McDonald, R. A.; Syverud, A. N. *J. Phys. Chem. Ref. Data* **1985**, *14* (1), 1179.
(28) Lutz, A. E.; Kee, R. J.; Miller, J. A. *SENKIN: A Fortran Program for Predicting Homogeneous Gas-Phase Chemical Kinetics With Sensitivity Analysis.* Sandia report SAND87-8248, Sandia National Laboratories: Livermore, CA, 1993.